Electronic and magnetic structure of Mn-Ni alloys in two and three dimensions

1999 J. Phys.: Condens. Matter 11 6359

(http://iopscience.iop.org/0953-8984/11/33/306)

J. Phys.: Condens. Matter **11** (1999) 6359–6372. Printed in the UK PII: S0953-8984(99)03747-9

Electronic and magnetic structure of Mn–Ni alloys in two and three dimensions

D Spišák and J Hafner

Institut für Materialphysik and Centre for Computational Materials Science, Universität Wien, A-1090 Vienna, Austria

Received 27 April 1999

Abstract. The electronic and magnetic structure of face-centred tetragonal Mn–Ni compounds and of structurally related c(2×2) Mn–Ni alloy films on Ni(001) substrates has been investigated using *ab initio* local-spin-density calculations including generalized gradient corrections. For the intermetallic compound a layered antiferromagnetic high-spin ground state with Mn moments of $\pm 3.2\ \mu_B$ (LSDA) and $\pm 3.4\ \mu_B$ (GGCs) and non-magnetic Ni atoms is predicted, in good agreement with the estimates from magnetic neutron scattering. Calculations of the magnetic anisotropy energy show that the moments are aligned in the Mn planes, parallel to the edges of the unit cell. An alloy with unit cell dimensions of the Mn–Ni planes strained to match the lattice parameter of the Ni(001) substrate has a very similar magnetic structure, albeit with slightly reduced moments. A monolayer c(2×2) Mn–Ni alloy shows high-spin ferromagnetic order ($\mu_{Mn} = 3.9\ \mu_B$). Films with two and more monolayers show antiferromagnetic interlayer coupling, with a quite pronounced enhancement of the surface moments over those in the deeper layers. The predicted antiferromagnetic ordering of the films emphasizes the similarity of the atomic and magnetic structures of the two-dimensional films with that of the three-dimensional compounds and contradicts recent claims as to a ferromagnetic order of the films not only in the monolayer limit. Possible explanations of this discrepancy are discussed.

1. Introduction

It is well known that the magnetic moment of transition-metal atoms can undergo large variations as a function of atomic structure and volume. Mn is a particularly interesting case for study because according to Hund's rule the magnetic moment of the free atom is as large as $5\ \mu_B$. In its various crystalline phases Mn assumes very different magnetic states: α-Mn crystallizes in a complex body-centred lattice and has a noncollinear magnetic ground state with magnetic moments varying between $-1.43\ \mu_B$ and $1.79\ \mu_B$ [1, 2], β-Mn has a complex simple cubic structure and is paramagnetic [1] and γ-Mn is face-centred cubic and has an antiferromagnetic low-spin state with $\mu \approx 0.6\ \mu_B$ at the equilibrium volume, undergoing a transition to a high-spin state with $\mu \approx 2.3\ \mu_B$ at a modest expansion [3–5]. Body-centred cubic δ-Mn is paramagnetic and hexagonal-close-packed Mn has a low-spin antiferromagnetic ground state according to local-spin-density calculations [3, 5]. Mn is also known to form strongly ferromagnetic compounds such as MnSb [6] and spin-glasses such as dilute CuMn alloys (where the local Mn moment may be as large as $4.9\ \mu_B$) [7]. Most transition-metal compounds with Mn, however, are antiferromagnetic such as MnPd, MnIr, MnRh, MnPt with a tetragonal CuAu I-type low-temperature phase, a disordered face-centred cubic high-temperature phase and an intermediate ordered CsCl phase [8]. The same crystal structures are also assumed by the equiatomic MnNi compounds, with the exception of the intermediate phase

0953-8984/99/336359+14$30.00

which assumes a disordered body-centred cubic structure [9]. The particular interest in the MnNi compounds is in interplay of the antiferromagnetism of Mn and the ferromagnetism of Ni. Neutron-diffraction investigations of Kasper and Kouvel [10] have shown that tetragonal MnNi where Mn and Ni occupy alternating planes perpendicular to the tetragonal axis has in-plane antiferromagnetism in Mn layers. Mn moments are estimated to be as large as 4 μ_B and oriented either along [100] or [110]; Ni moments are considerably lower than the 0.6 μ_B of ferromagnetic fcc Ni, indicating that the ferromagnetism of Ni is quenched by frustrated exchange interactions.

Recently the interest in the magnetism of Mn–Ni alloys was revived by the discovery of the complex structural and magnetic properties of Mn films on Ni(001) substrates [11–14]. At submonolayer coverage an ordered c(2×2) surface alloy is formed. The surface alloy shows considerable buckling and ferromagnetic order. It is important to note that the formation of the ordered surface alloy occurs only at deposition at temperatures above 270 K; at lower temperatures the diffusion processes necessary for the formation of a superstructure are kinetically hindered. At higher coverage the c(2×2) superstructure produced above a critical deposition temperature resembles closely the tetragonal phase of MnNi—hence an ordered intermetallic compound is grown epitaxially on a metal substrate [11]. In agreement with the scenario of a diffusion-limited growth process, the minimum deposition temperature for the growth of an ordered alloy layer increases with increasing thickness.

The magnetism of ordered c(2×2) MnNi/Ni(001) alloy layers in the monolayer regime has been characterized using x-ray magnetic circular dichroism (XMCD) and soft x-ray absorption spectroscopy (SXAS) [12, 13, 15]. It was concluded that Mn is in a ferromagnetic high-spin state with its moment oriented ferromagnetically to the Ni moment in the surface alloy and in the substrate. The existence of an Mn moment that is strongly enhanced compared to the bulk value in pure Mn is confirmed by photoemission (PES) and inverse photoemission (IPES) spectra [14] yielding an exchange splitting of $\Delta E = 5.25 \pm 0.2$ eV. First-principles electronic structure calculations [14] yield a magnetic moment of $\mu_{Mn} = 3.5\ \mu_B$, but an exchange splitting of only $\Delta E = 3.41$ eV. The ferromagnetism of c(2×2) MnNi/Ni(001) agrees with the well known ferromagnetic coupling of second-nearest-neighbour Mn atoms in most alloys.

The situation is less clear for thicker alloy layers. O'Brien and Tonner [12] concluded from XMCD measurements that in samples of 1, 2 and 4 monolayers thickness Mn is ferromagnetically ordered and aligned parallel to the moments in the Ni substrate. If it is assumed that the structure of the alloy layers corresponds to that of an epitaxially grown face-centred tetragonal MnNi phase, there is an evident conflict between the antiferromagnetism of the bulk compound and the ferromagnetism of the surface alloy.

In the present paper we report first-principles local-spin-density calculations of MnNi alloys in two and three dimensions and present a detailed analysis of the magnetic structure, anisotropy and exchange interactions.

2. Methodology

Our calculations have been performed using the scalar-relativistic real-space tight-binding linear-muffin-tin-orbitals (RS-TB-LMTO) technique described earlier [16, 17]. The two-centre local-spin-density Hamiltonian is expressed in a linear-muffin-tin-orbital basis

$$h^\alpha = c^\alpha - E_\nu + (d^\alpha)^{1/2} S^\alpha (d^\alpha)^{1/2} \tag{1}$$

where S^α is the screened structure constant matrix, E_ν is the reference energy for the linearization and c^α and d^α are the LMTO potential parameters (α is a shorthand notation for the screened tight-binding representation, the lattice site $\vec{R}_i$ and the quantum numbers n, l,

m, s) and transformed to a nearly orthonormal representation

$$H = E_v + h^\alpha - h^\alpha o^\alpha h^\alpha + \cdots \tag{2}$$

where o^α is the overlap matrix [18, 19]. The local densities of states (DOSs) are obtained using the real-space recursion method [20]. The local charge and spin densities are re-calculated from the moments of the densities of states.

For the calculation of the electronic contribution to the magnetic anisotropy energy (MAE) the spin–orbit coupling term is added to the scalar-relativistic Hamiltonian. The shape-anisotropy contribution to the MAE is calculated by Ewald summations of the magnetic dipole interactions on the converged configurations.

The exchange pair interactions J_{ij} are calculated using the Green function approach and the recursion technique presented earlier [21]

$$J_{ij} = \frac{\Delta_i \Delta_j}{2\pi} \operatorname{Im} \int^{E_F} \operatorname{Tr} G_{ij}^{\uparrow\uparrow}(E) G_{ij}^{\downarrow\downarrow}(E)\, \mathrm{d}E \tag{3}$$

where Δ_i is the local exchange splitting on the site $\vec{R}_i$ calculated in terms of the difference of the LMTO potential parameters representing the centre of gravity of the spin-up and spin-down bands. The mean field estimate of the local Curie temperature is related to the on-site exchange coupling J_{ii} via

$$T_{C,i} = \frac{1}{3k_B}\left(\frac{1}{2}\Delta_i \mu_i - J_{ii}\right). \tag{4}$$

The local critical temperature should be viewed as a measure of the local stability of the magnetic state of the atom at site i surrounded by all other atoms.

3. Bulk Mn–Ni alloys

In the low-temperature θ-phase MnNi crystallizes in the face-centred tetragonal CuAu I-structure with $a = b = 3.74$ Å and $c = 3.52$ Å. Mn and Ni atoms occupy alternating planes perpendicular to the tetragonal axis. The atomic and magnetic unit cells coincide; the magnetic moments of nearest-neighbour Mn atoms are antiparallel, $\mu_{Mn} \approx 4.0\ \mu_B$ according to Kasper and Kouvel [10], $\mu_{Mn} \approx 3.8 \pm 0.3\ \mu_B$ according to Kren *et al* [9]. The moments are aligned in the plane perpendicular to the tetragonal axis. The magnetic moments of the Ni atoms, if any exist, are smaller than $0.2\ \mu_B$.

The RS-TB-LMTO calculations have been performed for a supercell consisting of $6 \times 6 \times 6$ elementary cells, using 12, 20 and 40 recursion levels for s, p and d orbitals, respectively. We have searched for ferromagnetic as well as antiferromagnetic solutions (with in-plane antiferromagnetism in the layers perpendicular to the tetragonal axis). Our results are summarized in table 1. The antiferromagnetic solution is found to be 0.43 eV/atom energetically more favourable. The magnetic moments on the Mn sites are $\pm 3.19\ \mu_B$; the magnetism on the Ni sites is completely quenched by frustrated exchange interactions. In the ferromagnetic phase the Mn moment is slightly lower ($\mu_{Mn} = 2.90\ \mu_B$), but now the Ni atoms are also magnetic with a moment of $\mu_{Ni} = 0.48\ \mu_B$ that is only slightly lower than in bulk fcc Ni ($\mu_{Ni} = 0.62\ \mu_B$). The accuracy of the real-space approach has been checked by performing $\vec{k}$-space calculations for the antiferromagnetic phase (using 1183 $\vec{k}$-points in the irreducible part of the Brillouin zone). The $\vec{k}$-space approach yields almost the same magnetic moments for the Mn sites ($\mu_{Mn} = \pm\ 3.20\ \mu_B$), but also a small magnetic moment on the Ni sites ($\mu_{Ni} = \pm\ 0.22\ \mu_B$), showing the same type of antiferromagnetic in-plane ordering as in the Mn layers.

Table 1. Magnetic moments μ_{Mn}, μ_{Ni}, nearest-neighbour (n.n.) and next-nearest-neighbour (n.n.n.) Mn–Mn exchange interactions J_{Mn-Mn}, 'local' critical temperatures $T_{C,Mn(Ni)}$, anisotropy energy MAE $= E_{band}(100) - E_{band}(001)$ and magnetic energy difference $\Delta E_{mag} = E_{FM} - E_{AFM}$ for bulk MnNi (part (a)) and MnNi strained to match the structure of the Ni(001) substrate (part (b)), calculated in the LSDA and using GGCs.

	LSDA		CGA
	AFM	F	AFM
Bulk MnNi			
μ_{Mn} (μ_B)	± 3.19	2.90	± 3.37
μ_{Ni} (μ_B)	<0.01	0.48	<0.01
$J^{n.n.}_{Mn-Mn}$ (meV)	58.9	-129.7	60.1
$J^{n.n.n.}_{Mn-Mn}(x)$ (meV)	12.6	14.2	12.6
$J^{n.n.n.}_{Mn-Mn}(z)$ (meV)	18.0	21.5	19.2
$T_{C,Mn}$ (K)	2570	-720	2980
$T_{C,Ni}$ (K)	0	200	0
MAE (μeV)	-27		
ΔE_{mag} (meV)	430		
Strained MnNi			
μ_{Mn} (μ_B)	± 2.94	2.30	± 3.15
μ_{Ni} (μ_B)	± 0.09	0.31	± 0.01
$J^{n.n.}_{Mn-Mn}$ (meV)	61.8	-106.0	66.7
$J^{n.n.n.}_{Mn-Mn}(x)$ (meV)	10.8	7.4	11.1
$J^{n.n.n.}_{Mn-Mn}(z)$ (meV)	15.4	10.7	15.8
$T_{C,Mn}$ (K)	2690	-960	3140
$T_{C,Ni}$ (K)	10	80	10
MAE (μeV)	-46		
ΔE_{mag} (meV)	490		

The magnetic moments calculated in the local-spin-density approximation (LSDA) are lower than those estimated from experiment. For pure Mn it has been shown that non-local corrections to the exchange–correlation functional have a pronounced influence on the prediction of the cohesive and magnetic properties [4, 5]; adding generalized gradient corrections (GGCs) [22, 23] lifts the almost-degeneracy of the different structural and magnetic states, stabilizes a high magnetic moment at equilibrium density and yields a large magneto-volume effect. The influence is distinctly weaker in the MnNi alloy: at fixed lattice parameters, the GGCs lead only to a small enhancement of the Mn moments to $\pm 3.37\ \mu_B$. With this enhancement, the calculated magnetic moments are now almost within the range of the experimental uncertainty (considering the dependence of the analysis of the magnetic neutron scattering on the not very precisely known magnetic form factors).

The spin-polarized electronic density of states (DOS) is shown in figure 1. The most remarkable results are the formation of a very deep DOS minimum at the Fermi level (which makes MnNi almost a zero-gap semiconductor) and the localized nature of the Mn minority spin states located just above the Fermi level. The analysis of the DOS reveals that without the Ni atoms, Mn would be in this system in an atomic-like Hund-rule state with completely filled spin-up and empty spin-down states. However, the hybridization with the Ni states broadens the Mn majority-spin band and induces a resonance in the unoccupied Ni bands through the interaction with the empty localized Mn minority-spin-states.

We have also calculated the exchange pair interactions using the real-space recursion approach [21]. The results for nearest- and next-nearest-neighbour Mn–Mn interactions are

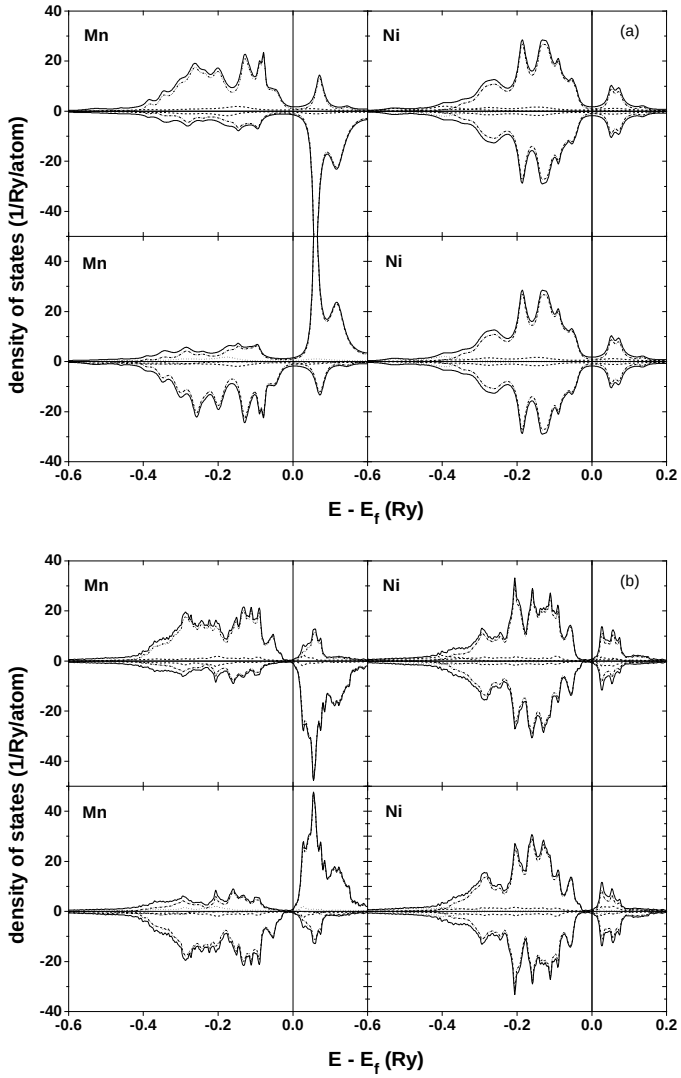

Figure 1. Total and angular-momentum decomposed spin-polarized densities of states of the face-centred tetragonal antiferromagnetic MnNi. Full line: total DOS, dotted lines: partial s-DOS, dashed lines: partial p-DOS, dot–dashed lines: partial d-DOS. Part (a) real-space recursion calculations, (b) $\vec{k}$-space calculation.

listed in table 1. Here we have adopted the convention that positive values of J_{ij} mean that for the given spin orientations the interactions are unfrustrated (i.e. the coupling is antiferromagnetic for n.n. and ferromagnetic for n.n.n. Mn pairs in AFM MnNi). We find that in the FM phase the nearest-neighbour coupling is very strongly frustrated, confirming the instability of the FM phase. The Mn–Ni exchange interactions are very weak in AFM MnNi ($|J_{ij}| \leqslant 8.8$ meV). Hence it is the coincidence of an FM Ni–Ni and Mn–Ni coupling with a strong AFM Mn–Mn n.n. coupling that leads to the quenching of the Ni magnetism in the AFM Mn–Ni alloy.

In a mean-field approximation, the local Curie temperature can be calculated from the on-site exchange interactions. For AFM MnNi this leads to a high local critical temperature

at the Mn sites; for FM MnNi the frustrated interactions lead to the prediction of a negative local Curie temperature emphasizing the instability of the ferromagnetic configuration.

Finally we have calculated the magnetic anisotropy energy MAE $= E(100) - E(001)$ defined as the energy difference for magnetic moments oriented perpendicular and parallel to the tetragonal axis by adding the spin–orbit coupling term and using the force theorem stating that the total energy difference is approximated by the difference in the band energies calculated for a fixed potential. In accordance with experiment we find MAE $= -27.2$ μeV/atom, i.e. a preference for an orientation of the moments within the Mn layers and perpendicular to the tetragonal axis. We have also attempted to calculate the in-plane MAE, defined as $E(110) - E(100)$. The in-plane MAE is found to be 2.2 μeV/atom, i.e. we predict an orientation of the moments along edges of the tetragonal cell. Again this agrees with experiment, but we should be honest enough to point out that such exceedingly small energy differences are at the limit of the accuracy of such calculations.

4. Strained Mn–Ni alloys

To achieve an epitaxial relationship between an Mn–Ni alloy layer and the Ni(001) substrate with an in-plane lattice constant of 3.52 Å, the structure of face-centred tetragonal MnNi must be strained such that $a = 3.74$ Å and $b = c = 3.52$ Å, i.e. the lattice is compressed along the b-axis. In the layers along the a-axis parallel to the surface of the substrate we have now a perfect c(2×2) structure (see figure 2). We have repeated the calculations for this strained MnNi structure; the results are given in table 1. Due to the reduced in-plane Mn–Mn distances, the Mn moments are reduced in both the AFM and FM phases compared to the strain-free lattice. In the stable AFM phase the antiferromagnetic n.n. interactions are slightly enhanced, whereas the ferromagnetic n.n.n. interactions are reduced, the frustration of the exchange coupling in the FM phase is even more pronounced. Magnetic energy differences and axial MAE are even larger than in the unstrained structure.

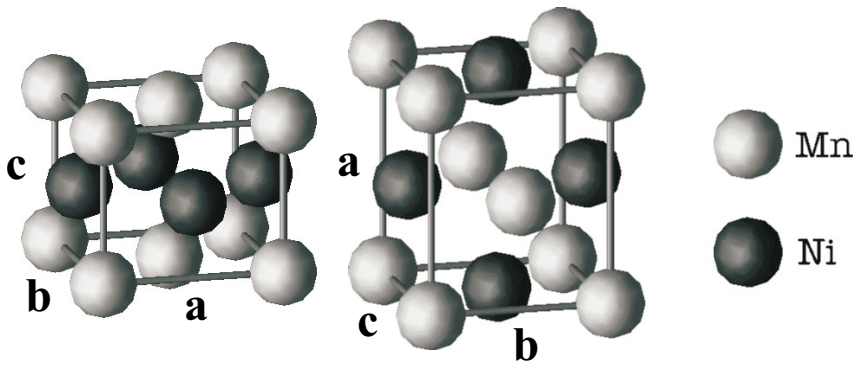

Figure 2. Face-centred tetragonal structure of bulk MnNi (left, $a = b = 3.74$ Å, $c = 3.52$ Å) and the strained structure matching the Ni(001) substrate (right, $a = 3.74$ Å, $b = c = 3.52$ Å).

5. Mn–Ni alloy films on Ni(001)

In the following we present a detailed analysis of the magnetism of MnNi-alloy layers grown on Ni(001). The low-energy diffraction (LEED) studies of Wuttig *et al* [11] have shown that films deposited at temperatures higher than a certain critical temperature form ordered alloys

with a c(2×2) structure compatible with that of the strained fct MnNi structure described in the preceding section. The maximum thickness of the ordered alloy films depends critically upon the actual growth temperature. Above this maximum thickness kinetic limitations lead to an excess of Mn at the surface and in consequence to the formation of superstructures depending on the Mn/Ni concentration. Here only c(2×2) alloys will be considered.

The LEED studies also revealed a considerable buckling of the surface layer; Mn atoms relax outward by about 0.25 ± 0.02 Å compared to the Ni atoms, presumably because of a magneto-volume effect. Similar reconstructions were also reported for c(2×2) CuMn/Cu(001) surface alloys [24]. *Ab initio* local-spin density calculations have demonstrated that the outward relaxation of the Mn atoms is directly related to the formation of a high-spin state and a pronounced local magneto-volume [25, 26]. In the present study we concentrate on the magnetic properties and use the relaxed surface structure determined experimentally (with the outwardly relaxed Mn atoms in the top layer) in all calculations. The calculations are performed for a model consisting of three vacuum layers, one to four alloy layers and ten Ni layers. The c(2×2) surface cell is periodically repeated in the lateral directions, leading to a supercell containing between about 2000 and 2600 atoms depending on the thickness of the MnNi-alloy film. Along the axis perpendicular to the surface the free boundary conditions were used. 20, 20 and 50 recursion levels were used in the RS-TB-LMTO calculations for s, p and d orbitals, respectively.

5.1. Magnetic structure

For the coupling between the Ni substrate and the first MnNi layer a ferromagnetic alignment was assumed (an antiparallel alignment always leads to frustrated interactions). For two and more monolayers different FM and AFM orientations of the moments have been examined. The results are compiled in table 2. In any case an antiferromagnetic layer sequence is energetically more favourable: $\downarrow\uparrow$ for 2 ML, $\uparrow\downarrow\uparrow$ for 3 ML and $\downarrow\uparrow\downarrow\uparrow$ for 4 ML; for 4 ML films no converged FM solution could be found. The Mn atoms in the top layer are always in a high-spin state with $\mu_{Mn} \approx \pm 3.9\ \mu_B$, in the deeper alloy layers the Mn moments decrease to 2.8–3.0 μ_B. In the FM 1 ML MnNi/Ni(001) alloy the Ni moments are slightly reduced in the alloy layer and at the top layer of the substrate compared to their value in bulk fcc Ni. A similar situation also holds in the thicker FM layers. For an AFM configuration, the Ni moments in the alloy layers are strongly reduced. This happens especially in the interior of the films, whereas a weak Ni moment survives at the surface and at the interface. For the 4 ML film, the magnetic moments in the interior of the film are already quite well converged to the values characteristic for the strained fct MnNi lattice. Because of the antiparallel orientation of the magnetic moments in the neighbouring layers, films with an odd number of monolayers show a substantial global magnetization parallel to that of the Ni substrate (and hence should be characterized as ferrimagnetic). Films with an even number of monolayers on the other hand show only a very small total magnetization—generally with an orientation opposite to that of the substrate because of surface-induced enhancement of the moments in the top layers and the ferromagnetic Mn–Ni coupling at the interface.

The instability of a ferromagnetic layer sequence is also confirmed by the analysis of the exchange pair interactions (table 3). The ferromagnetic next-nearest-neighbour coupling between Mn atoms within the same layer is much weaker than in the bulk for films with only one or two monolayers. The nearest-neighbour coupling between Mn atoms in adjacent layers with antiparallel orientation of the moments is also reduced compared to the bulk close to the surface, but reaches bulk-like values in the deeper layers of the films. For ferromagnetic coupling between the layers the nearest-neighbour Mn–Mn exchange interactions are very

Table 2. Layer resolved magnetic moments μ_i and average moments $\bar{\mu}_{Mn}$ in the MnNi/Ni(001) system (in μ_B). Mn moments are printed boldface. ΔE_{mag} lists the magnetic energy difference relative to the ground state (in MeV/atom).

	↑	↓↑	↑↑	↑↓↑	↓↓↑	↑↑↑	↓↑↓↑	↑↑↓↑
ΔE_{mag}	0	0	39	0	50	69	0	63
μ_{11}	**3.86**	**−3.83**	**3.87**	**3.86**	**−3.92**	**3.87**	**−3.73**	**3.87**
μ_{12}	0.41	−0.16	0.55	0.20	−0.49	0.54	−0.20	0.50
μ_{21}	0.46	**3.09**	**3.02**	**−3.01**	**−2.90**	**2.79**	**2.95**	**2.88**
μ_{22}	0.46	0.27	0.41	−0.10	−0.28	0.44	0.08	0.32
μ_{31}	0.66	0.48	0.53	**2.87**	**2.81**	**2.72**	**−2.82**	**−2.75**
μ_{32}	0.67	0.49	0.54	0.19	0.17	0.48	−0.01	0.04
μ_{41}	0.67	0.66	0.64	0.50	0.50	0.55	**2.94**	**2.94**
μ_{42}	0.67	0.65	0.63	0.41	0.40	0.52	0.29	0.29
μ_{51}	0.64	0.64	0.65	0.64	0.63	0.63	0.59	0.59
μ_{52}		0.67	0.65	0.63	0.64	0.62	0.45	0.46
μ_{61}		0.65	0.65	0.62	0.62	0.65	0.67	0.67
μ_{62}				0.67	0.67	0.64	0.65	0.66
μ_{71}				0.64	0.64	0.65	0.65	0.66
μ_{72}							0.68	0.68
μ_{81}							0.67	0.67
$\bar{\mu}_{Mn}$	**3.86**	**−0.37**	**3.45**	**1.24**	**−1.34**	**3.13**	**−0.16**	**1.74**

Table 3. Exchange pair interactions J_{ij} between Mn atoms in the MnNi/Ni(001) alloy films and Mn–Ni interactions across the film interface (in meV). Numbers in parentheses stand for the layer index. Cf text.

	↑	↓↑	↑↑	↑↓↑	↓↓↑	↑↑↑	↓↑↓↑	↑↑↓↑
Mn(1)–Mn(1)	2.9	7.4	9.7	9.4	14.4	11.5	11.8	10.4
Mn(1)–Mn(2)		32.5	−43.2	27.8	−31.4	−50.3	42.5	−54.4
Mn(2)–Mn(2)		9.6	12.1	13.1	16.1	24.6	13.7	19.1
Mn(2)–Mn(3)				77.4	86.7	−147.4	64.0	77.4
Mn(3)–Mn(3)				10.5	11.0	13.0	13.4	13.8
Mn(3)–Mn(4)							66.1	62.7
Mn(4)–Mn(4)							10.3	10.2
interface Mn–Ni	3.5	3.6	3.9	2.4	2.5	4.0	3.0	2.9

strongly frustrated, indicating the local instability of ferromagnetic configurations. The Mn–Ni interactions within the alloy layers are generally very weak ($|J_{ij}| \leqslant 4$ meV), Ni–Ni interactions even weaker ($|J_{ij}| \leqslant 1$ meV). The Mn–Ni interactions across the film–substrate interface are ferromagnetic, but rather weak. As for the bulk alloys, the local critical temperatures at the Mn sites calculated for the FM configurations are negative, confirming the instability of a ferromagnetic coupling between layers.

Our result of an antiferromagnetic (or, more precisely, ferrimagnetic) character of MnNi-alloy films on Ni(001) stands in apparent contradiction to the conclusions of O'Brien and Tonner [12] based on analysis of XMCD spectra for films with 1, 2 and 4 monolayer thickness. By comparing the relative sign of the Ni and Mn XMCD spectra they found that Mn is aligned ferromagnetically with the Ni substrate. However, no estimate of the magnetization of the alloy films was given. The conclusion that the global Mn magnetization in the films is parallel to the magnetization of the substrate agrees with our conclusions for the ferrimagnetic films with an odd number of monolayers, but disagrees for films with an even number of layers.

The apparent contradiction could possibly be resolved by considering the morphology of the films. If the surface is not atomically flat, the presence of steps would mean that parts of the film have always an odd number of layers, even if the average coverage corresponds to an even number of layers. In such a case, the correct sign of the Mn and Ni XMCD spectra would be obtained in any case, but the amplitude would depend on coverage and morphology. This point certainly needs further investigation.

5.2. Electronic structure

Figure 3 shows the layer-resolved spin-polarized local electronic densities of states for a monolayer of MnNi on Ni(001). The results demonstrate the large exchange splitting corresponding to the FM high-moment state of Mn in the alloy layer and the localized character of the Mn minority-spin states. The Ni DOS in the alloy layer reveals the characteristic band-narrowing resulting from the reduced Ni–Ni coordination. In the interface layer the Ni DOS for the minority spins lacks the characteristic sharp maximum at the upper band-edge which develops only in the deeper layers. This is again related to the reduction of the Ni moments at the interface.

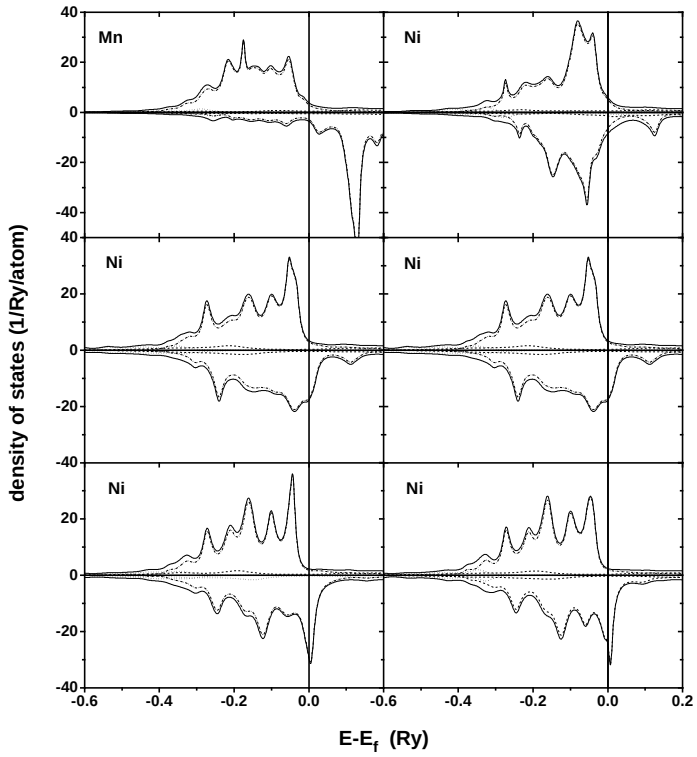

Figure 3. Spin-polarized electronic densities of states for 1 ML MnNi/Ni(001). Top row: alloy layer, middle row: top layer of the substrate, bottom row: second layer of the substrate. Full line: total DOS, dotted lines: partial s-DOS, dashed lines: partial p-DOS, dot–dashed lines: partial d-DOS.

As an example for the electronic spectra of the thicker alloy layers, the results for a 4 ML AFM MnNi/Ni(001) alloy film are shown in figure 4. The Mn DOS in all alloy layers is now quite similar to that of bulk fct MnNi, showing in particular the deep pseudogap at the

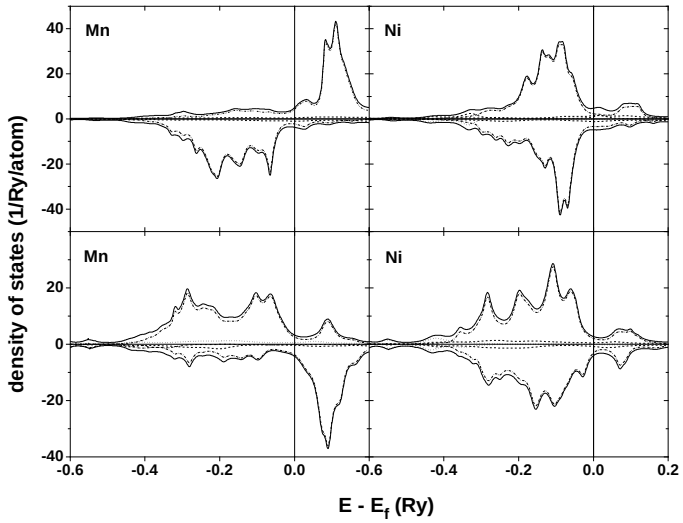

Figure 4. Spin-polarized electronic densities of states for an AFM 4 ML MnNi/Ni(001) alloy film. Surface and sub-surface layers are plotted. Same symbols as in figures 1 and 3. Cf text.

Fermi level in both the majority and minority bands. Only at the interface the Mn majority band is somewhat broadened through interaction with the Ni d band and the pseudogap is slightly smeared out. The narrowing of the Ni DOS is particularly pronounced in the top layer of the alloy film. In the interior of the film a pseudogap at the Fermi level opens up also in the Ni DOS, again in close analogy to the bulk fct MnNi. The spectra are very similar in all antiferromagnetic alloy films, independent of thickness.

The electronic DOS of ferromagnetic alloy films shows a very different character (see figure 5; only the Mn DOS is shown). Only the Mn atoms in the surface have a DOS reminiscent of that of the antiferromagnetic films; in the deeper layer we find a high DOS at the Fermi level in both majority- and minority-spin bands, illustrating the instability of a ferromagnetic configuration from an electronic point of view.

For the 1 ML MnNi/Ni(001) surface alloy our results may also be compared with the photoemission and inverse photoemission experiments of Rader *et al* [14]. The PES and IPES intensities may be approximated by the sum over the local partial DOS, weighted with the photoemission intensities of Yeh and Lindau [27]. The weighting of substrate and overlayer contributions depends of course critically upon the assumed escape (penetration) depth of the electrons. Figure 6 presents a comparison of the calculated and measured PES and IPES spectra, supposing that the ten top layers contribute to the photoelectron yield and to the emitted photon beam, respectively. To obtain the theoretical PES intensity, the partial local DOSs have been multiplied with the partial photoionization cross-sections, multiplied with a Fermi function and convoluted with a Gaussian of width 0.27 eV to account for the experimental resolution. In the calculation of the IPES intensity we proceeded accordingly. The comparison with experiment is hampered by the fact that the large background intensity increasing for the energies lower than -3 eV has not been subtracted. Nevertheless, we find a good agreement between theory and experiment: the dominant peak close to the Fermi level is due to Ni 3d states, mostly minority states. We believe that the agreement is even better than suggested by figure 6: the low PES at E_F is incompatible with the high minority DOS at E_F that is surely present in the Ni substrate. If the experimental curve is adjusted accordingly, the peaks match

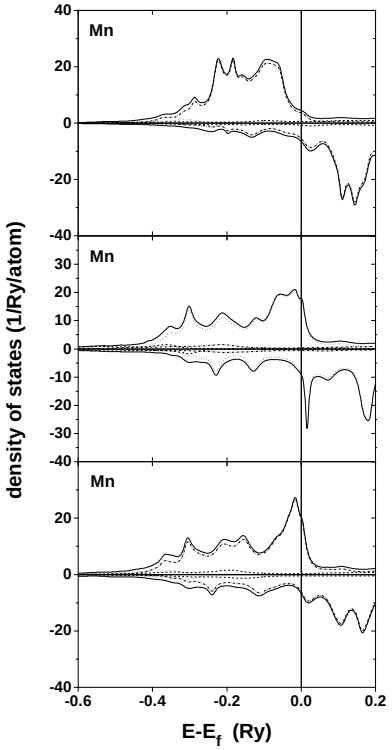

Figure 5. Spin-polarized electronic densities of states in an FM 3 ML MnNi/Ni(001) alloy film. Only the local Mn DOSs are shown. Same symbols as in figures 1 and 3.

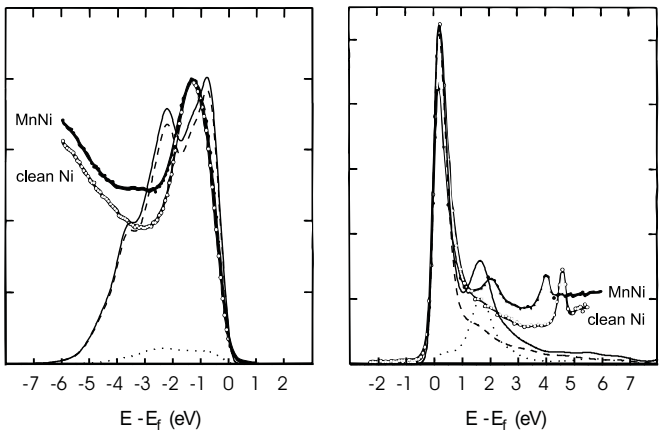

Figure 6. Measured (connected points) and calculated (total: full lines, Mn: dotted lines, Ni: dashed lines) PES (left) and IPES (right) intensities for 1 ML MnNi/Ni(001). No background subtraction has been made in the measured spectra.

perfectly. The maximum contribution from Mn is found around the centre of gravity of the Mn 3d band at −2.25 eV. The precise position of the Mn maximum is difficult to estimate from the angle-integrated spectra, but from angular-resolved photoemission spectroscopy, Rader *et al* determined the position of the centre of the Mn majority band at −3.2 eV.

In the IPES intensity we find a good agreement for the Ni-dominated states just above E_F; the peak associated with the localized Mn minority states is shifted to lower energies compared to experiment. The image-potential states at 4–5 eV are not reproduced, because our TB-LMTO calculations do not include a sufficient number of vacuum layers to grasp these states concentrated ≈4–5 Å above the surface (for a detailed discussion of image-potential states at the Ni(001) surface within the LSDA see, e.g., Mittendorfer *et al* [28].)

In relation to the magnetic properties, the most important features are in the PES intensity the maximum contribution from Mn at about -2.25 eV and in the IPES the main Mn peak situated at about 1.5 eV. As the DOSs are completely spin split, this gives directly an exchange splitting of $\Delta E = 3.75$ eV. Comparing the calculated moment of $\mu_{Mn} = 3.86\,\mu_B$, we arrive at a Stoner factor $I = 0.97$ eV μ_B (defined as $\Delta E = I\mu_{Mn}$) suggesting an itinerant character of the Mn magnetism. Our result for the exchange splitting agrees rather well with the full potential linearized augmented plane wave (FLAPW) calculations of Rader *et al*, yielding $\mu_{Mn} = 3.5\,\mu_B$ and $\Delta E = 3.41$ eV (LSDA results only). The small remaining differences are to be attributed to the fact that Rader *et al* used a thinner slab of only 9 ML and determined the surface buckling by a total-energy minimization. Experimentally an exchange splitting of $\Delta E = 5.25$ eV has been found, resulting from a shift of the centre of both spin-up and spin-down bands away from the Fermi level compared to the theoretical prediction ($E_\uparrow = -3.2$ eV (exp.), -2.25 eV (theor.), $E_\downarrow = 2.05$ eV (exp.), 1.5 eV (theor.)).

The simplest explanation for the discrepancy between theory and experiment is that the theory provides the difference in the eigenvalues for the neutral ground state. Both PES and IPES experiments create positively (negatively) charged ionized states. The additional Coulomb interaction lowers the hole state produced in the PES and increases the energy of the excited electron states produced in IPES. The effect is stronger for narrow bands representing states of localized character.

Unfortunately, no spectroscopic data for thicker alloy layers are available. Considering the different character of the DOS for the FM and AFM alloy films, this could be an important contribution toward understanding the true magnetic structure. For the AFM films one should see a strongly reduced DOS around E_F in both PES and IPES (cf figures 4 and 1), while in the FM films an appreciable DOS is expected in both spectra.

6. Conclusions

We have presented detailed local spin-density investigations of the electronic and magnetic properties of tetragonal MnNi compounds and of structurally closely related c(2×2) MnNi-alloy films on Ni(001) substrates. For the three-dimensional intermetallic compound our calculations yield a high-moment antiferromagnetic ground state with Mn moments aligned in the Mn planes parallel and antiparallel to the edges of the square face of the unit cell. This corresponds in detail to the magnetic structure deduced from the neutron-scattering studies [9, 10]. Ni moments are found to be completely quenched because of the conflict between the Ni–Ni and Mn–Ni exchange interactions. To obtain quantitative agreement with the measured Mn moment, gradient corrections to the exchange–correlation functional must be included. An interesting prediction is the formation of a very deep pseudo-gap at the Fermi level—this would certainly merit experimental verification. For the alloy layers with a c(2×2) structure corresponding to a strained version of the crystal structure of bulk MnNi, we find in the 1 ML limit a ferromagnetic state in good agreement with both magnetic measurements and electron spectroscopy. For two and more monolayers, however, we predict an antiferromagnetic alignment of the successive c(2×2) MnNi layers—in contrast to what has been deduced from the XMCD measurements. However, as the XMCD experiment

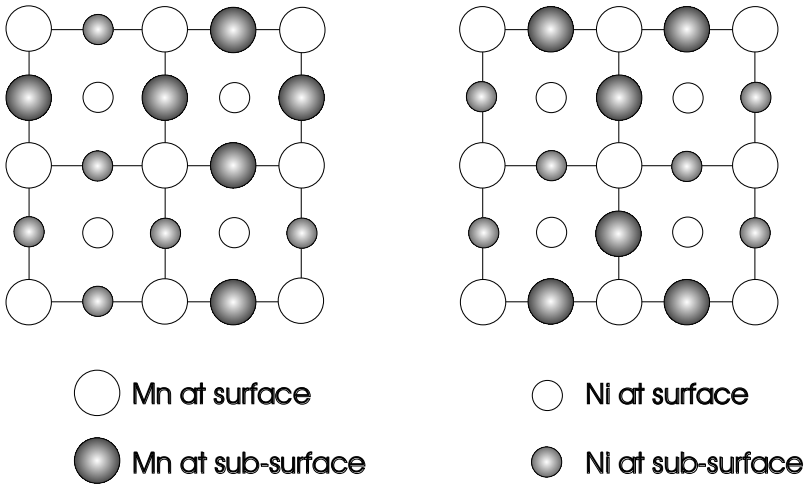

Figure 7. Supercells showing different disordered Mn–Ni distributions in the sub-surface layers. Cf text.

measures only the average Mn moment this argument is not necessarily complete; for films with an odd number of monolayers, the compensation of the antiparallel Mn moments is never complete and the residual Mn moment is always aligned parallel to the moments in the Ni substrate—this would agree with the XMCD experiment. For films with an even number of monolayers, the compensation of the moments is almost complete, and our results for perfect, atomically flat 2 ML and 4 ML films are difficult to reconcile with the experimental results. However, admitting a certain rugosity of the films would reconcile theoretical and experimental results.

We have also examined the possibility whether a chemical disorder in the deeper layers of the alloy films below an ordered c(2×2) top layer would allow for a ferromagnetic interlayer coupling. The supercells of two such configurations are shown in figure 7. The result was invariably that a broken c(2×2) order causes strong magnetic frustrations and is energetically unfavourable. This is a confirmation of the fact that the c(2×2) ordering is magnetically stabilized.

In summary, the present work demonstrates that *ab initio* local-spin-density studies are a very valuable tool for exploring the magnetic structure of complex materials such as thin alloy films. The results that we have obtained for the three-dimensional bulk alloys and for the monolayer films show that the theoretical predictions reliable and quantitatively accurate. This lends credibility to the results obtained for the thicker films which at a first glance are in contradiction to experiment. However, whereas the experiment measures only an average magnetic signal, the more detailed information available from the first-principle calculations allows the development of a scenario capable of reconciling theory and experiment.

Acknowledgment

This work has been supported by the Austrian Ministry for Science and Transport within the project ‘Magnetism on the nanometre scale’.

References

[1] Sliwko V, Mohn P and Schwarz K 1994 *J. Phys.: Condens. Matter* **6** 6557
[2] Endoh Y and Ishikawa Y 1973 *J. Phys. Soc. Japan* **30** 1614
[3] Zheng-Johansson J, Eriksson O, Johannson B, Fast L and Huja R 1998 *Phys. Rev.* B **57** 10 989
[4] Asada T and Terakura K 1993 *Phys. Rev.* B **47** 15 992
[5] Eder M, Moroni E G and Hafner J to be published
[6] Cade N A and Young W 1980 *J. Phys. F: Met. Phys.* **10** 2035
[7] Cohen J D and Slichter C P 1980 *Phys. Rev.* B **22** 45
[8] Daams J L C, Villars P and van Vucht J H N 1991 *Atlas of Crystal Structure Types for Intermetallic Phases* (Metals Park, OH: American Society for Metals)
[9] Kren E, Nagy E, Nagy I, Pál L and Szabó P 1968 *J. Phys. Chem. Solids* **29** 101
[10] Kasper J S and Kouvel J S 1959 *J. Phys. Chem. Solids* **11** 231
[11] Wuttig M, Flores T and Knight C C 1993 *Phys. Rev.* B **48** 12 082
[12] O'Brien W L and Tonner B P 1995 *Phys. Rev.* B **51** 617
[13] Schmitz D, Rader O, Carbone C and Eberhardt W 1996 *Phys. Rev.* B **54** 15 352
[14] Rader O *et al* 1997 *Phys. Rev.* B **55** 5404
[15] van der Laan G and Thole B T 1991 *Phys. Rev.* B **43** 13 401
[16] Lorenz R and Hafner J 1996 *Phys. Rev.* B **54** 15 397
[17] Spišák D and Hafner J in preparation
[18] Andersen O K and Jepsen O 1984 *Phys. Rev. Lett.* **53** 2571
[19] Andersen O K, Jepsen O and Šob M 1987 *Electronic Band Structure and its Applications (Lecture Notes in Physics 283)* ed M Youssouff (Berlin: Springer) pp 1–57
[20] Haydock R, Heine V and Kelly M J 1975 *J. Phys. C: Solid State Phys.* **8** 2591
[21] Spišák D and Hafner J 1997 *J. Magn. Magn. Mater.* **168** 257
[22] Perdew J P and Wang Y 1992 *Phys. Rev.* B **45** 13 244
[23] Perdew J P, Vosko S H, Jackson L A, Pedersen M R, Singh D J and Fiolhais C 1992 *Phys. Rev.* B **46** 6671
[24] Flores T, Hansen M and Wuttig M 1992 *Surf. Sci.* **279** 251
[25] Wuttig M, Gauthier Y and Blügel S 1993 *Phys. Rev. Lett.* **70** 3619
[26] Eder M, Hafner J and Moroni E G 1999 *Surf. Sci.* **423** L244
[27] Yeh J J and Lindau I 1985 *At. Data Nucl. Data Tables* **32** 1
[28] Mittendorfer F, Eichler A and Hafner J 1999 Surf. Sci. **423** 1